OPEN ACCESS
Journal of Innovative Optical Health Sciences
Vol. 16, No. 1 (2023) 2230018 (19 pages)

DOI: 10.1142/S179354582230018X

World Scientific
www.worldscientific.com

Nonlinear optical microscopy for skin *in vivo*: Basics, development and applications

Jianhua Zhao, Yuan Zhao, Zhenguo Wu, Yunxian Tian and Haishan Zeng*
Integrative Oncology Department – Imaging Unit
BC Cancer Research Institute, Vancouver, BC, Canada

Department of Dermatology and Skin Science
University of British Columbia and
Vancouver Coastal Health Research Institute
Vancouver, BC, Canada
**hzeng@bccrc.ca*

Received 30 September 2022
Accepted 17 November 2022
Published 9 February 2023

Multi-photon microscopy (MPM) and coherent anti-Stokes Raman scattering (CARS) are two advanced nonlinear optical imaging techniques, which provide complementary information and have great potential in combination for noninvasive *in vivo* biomedical applications. This paper provides a detailed discussion of the basics, development and applications of these technologies for *in vivo* skin research, covering the following topics: The principle and advantage of MPM and CARS, instrumentation development for *in vivo* applications, MPM and CARS of normal skin, application of MPM and CARS in skin cancer and disease diagnosis; application of MPM in skin disease intervention, i.e., imaging guided two-photon photothermolysis.

Keywords: Nonlinear microscopy; multiphoton microscopy; coherent anti-Stokes Raman scattering microscopy; skin; skin cancer; multiphoton therapy.

1. Introduction

Multi-photon microscopy (MPM) is a nonlinear optical imaging technique based on multi-photon absorption. Since its inception about three decades ago by Webb *et al.*,[1] it has been widely used in a number of fields, including molecular biology,[1–3] cellular biology,[4,5] tissue biology,[6,7] neuron science,[8–15] developmental science,[16] skin science[17–23] and immunology.[24–27] Coherent anti-Stokes Raman scattering (CARS) is another nonlinear optical imaging technique which can provide complementary chemical information.[28–30] It has been proven that CARS is particularly useful for imaging nonfluorescent biological molecules such as mapping lipid compartments, protein clusters and water distributions in cell tissue cultures.[31–33] Currently, the

*Corresponding author.

state-of-the-art CARS microscopy has high enough sensitivity to detect single lipid bilayers.[34,35] It has been used for *in vivo* studies of mouse skin[36] and human skin.[37] In this paper, we will present the basics, development and applications of MPM and CARS technology for *in vivo* skin research. It is structured as follows: Principle and advantage of MPM and CARS; instrumentation development for *in vivo* applications; MPM and CARS of normal skin; application of MPM and CARS in skin cancer and disease diagnosis; application of MPM in skin disease intervention, i.e., imaging guided two-photon photothermolysis.

1.1. *Principle of MPM*

The principle of MPM can be illustrated by a simplified Jablonski diagram, as shown in Fig. 1(a). In the process of conventional single photon excitation fluorescence (SPF), the molecule in the ground state absorbs a single photon (ω) and is excited to a singlet state. The molecule in the singlet state is unstable. It drops back to the lowest energy level of the excited state after some internal thermal relaxation and then returns to ground state by emitting a new photon (in a time scale of nanosecond). The newly emitted photon usually has lower energy than the incident photon ($\omega' < \omega$). The SPF intensity is linearly dependent on the excitation light intensity. The process of two-photon excitation fluorescence (TPF) is similar to that of SPF, but instead of absorbing a single photon, the molecule in the ground state needs to absorb two photons (2ω) simultaneously (in a time scale of 10^{-15} sec) in order to be excited to the singlet state. The emitted photons in TPF usually have lower energy than the total energy of the two incident photons ($\omega' < 2\omega$). For some noncentrosymmetric molecules such as collagen or muscles,[38–43] there is a second harmonic generation (SHG) process, in which the molecule in the ground state is excited to a virtual state by "scattering" two photons simultaneously. In the process of SHG, the emitted photon has energy exactly twice of the excitation photon ($\omega' = 2\omega$). The TPF intensity and the SHG intensity have a nonlinear, quadratic dependence on the excitation intensity. Similarly, molecules in the ground states can absorb simultaneously three photons and generate three-photon fluorescence ($\omega' < 3\omega$) or third harmonic generation signals ($\omega' = 3\omega$).[44] The lifetimes of different fluorophores also vary, which provides the contrast for time-resolved fluorescence lifetime imaging (FLIM). Two-photon-based FLIM has been used to study a number of skin conditions.[45–48]

1.2. *Principle of CARS*

The principle of CARS can be illustrated by a simplified Jablonski diagram, as shown in Fig. 1(b) including spontaneous Raman scattering. Different from fluorescence which measures the absorption properties of molecules in the singlet states, both spontaneous Raman and CARS measure the molecular vibrations at the ground state (ΔE_{vib} in Fig. 1(b)). Spontaneous Raman scattering is a single-photon process, where the Raman signal

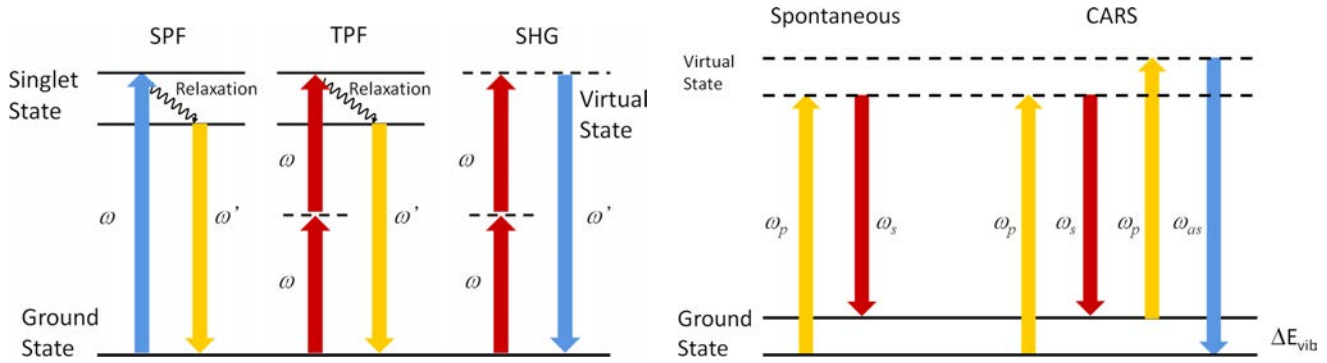

Fig. 1. Jablonski diagram for MPM (a) and CARS (b) process, including single-photon fluorescence (SPF), two-photon fluorescence (TPF), second harmonic generation (SHG), spontaneous Raman scattering and CARS. ω and ω' represent excitation and emission beam in MPM process. ω_p, ω_s and ω_{as} represent pump, Stokes and anti-Stokes beam in CARS process. ΔE_{vib}: Energy difference between two sub-states. Dashed line represents virtual state. MPM: Multi-photon microscopy. CARS: Coherent anti-Stokes Raman scattering.

intensity is linearly dependent on the excitation intensity (I_p), while CARS is a four-wave mixing process, which requires a pump beam (ω_p) and a Stokes beam (ω_s). When the Raman shift ω_p–ω_s is tuned to be resonant with a given vibrational mode (ΔE_{vib}), a resonantly enhanced CARS signal (ω_{as}) is observed at the anti-Stokes frequency of $2\omega_p$–ω_s in the phase matching direction. The wavelength of CARS is blue-shifted with respect to the pump and the Stokes beams. CARS intensity is quadratically dependent on the excitation (pump) intensity, given in Refs. 28 and 30: $I_{\text{CARS}} \propto |\chi^{(3)}|^2 I_p^2 I_s$, where I_p and I_s are the intensity of the pump and Stokes beams, $\chi^{(3)}$ is the third-order nonlinear susceptibility. $\chi^{(3)}$ has one resonant term $\chi_R^{(3)}$ and one nonresonant term $\chi_{\text{NR}}^{(3)}$, given by $\chi^{(3)} = \chi_{\text{NR}}^{(3)} + \frac{\chi_R^{(3)}}{\Delta - i\Gamma}$ where Δ is the frequency detuning: $\Delta = \omega_P - \omega_s - \Omega_R$, and Ω_R is the center frequency of a homogenously broadened Raman line with bandwidth Γ. It is difficult if not impossible to implement background-free CARS signal due to the nonresonant term.

1.3. *Advantages and limitations of MPM and CARS*

MPM relies on contrast of TPF and SHG; CARS relies on molecular vibrations; therefore both modalities provide complementary information. The advantages and limitations of these techniques are summarized in Table 1. The major advantages are as follows:

(i) Both modalities are not affected by the fluorescence background that is associated with SPF or spontaneous Raman process because the MPM or CARS signals are on the shorter wavelength side of the excitation beam;

(ii) The excitation for MPM and CARS is usually in the near infrared range (700–1500 nm), which is much less scattered or absorbed than shorter excitation wavelengths in single-photon excitation process, therefore it is possible to implement deep tissue imaging[49];

(iii) Both modalities are inherently depth-resolved without the need for a multi-scattering light-rejecting confocal pinhole because they require absorption or scattering of multi-photons simultaneously in the focal volume;

(iv) Concurrently, because there is no limiting pinhole in none descanned MPM or CARS system, the signal is much stronger and the acquisition time is much shorter than confocal configuration[21];

(v) Because the intensity of TPF and CARS is quadratically dependent on the excitation (pump beam for CARS), both modalities have higher signal-to-noise ratio and less photo damage compared to their respective single-photon excitation process.[30] However, they all also have their own respective limitations: MPM is affected by the photobleaching effect at the focal point; CARS is limited by the background due to the nonresonant term in the susceptibility. Both techniques also require complicated and costly laser sources and system setups.

2. Instrumentation and Characterization of MPM and CARS for *In Vivo* Applications

2.1. *Instrumentation*

A typical MPM or CARS system can be schematically illustrated in Fig. 2. It is typically composed of

Table 1. Advantages and limitations of MPM and CARS.

Properties	MPM	CARS
Imaging contrast	TPF, SHG	Molecular vibrations
Fluorescence background	Not affected	Not affected
Imaging depth	Deep	Deep
Depth-resolved capability	Yes	Yes
Photobleaching effect	Affected	Not affected
Photodamage effect	Low	Low
Compared to confocal configuration	Higher signal-to-noise ratio	Higher signal-to-noise ratio
Laser source	Near-infrared single laser source	Near-infrared sophisticated light source
Cost	High	High
Background	Free	Not free due to nonresonant term

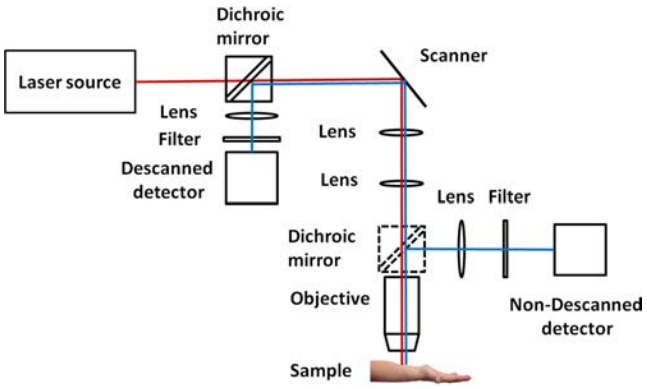

Fig. 2. Block diagram of a typical descanned and nondescanned MPM/CARS system. In descanned MPM/CARS system, the detector is placed behind the scanner. The position of the signal beam on the detector does not move during the scanning process. In nondescanned MPM/CARS system, the detector is placed right behind the objective (in front of the scanner). The position of the signal beam on the detector moves according to the scanning pattern. A large-area detector is required in nondescanned MPM/CARS system. The telescope lenses are used to expand the scanning beam which overfills the back aperture of the objective in order to fully use the numeric aperture of the objective. The two dichroic mirrors are used to separate the excitation beam and the signal beam. The two dichroic mirrors are not used at the same time as indicated by dashed and solid lines, respectively.

a laser source, an x-y scanner, an objective and a photo-multiplier tube (PMT) or an avalanche photodiode (APD) detector. Depending on the location of the detectors, it can be divided into descanned and nondescanned systems. A descanned system has the detector located after the x-y scanners, which is equivalent to a confocal microscope. The image of the signal on the detector does not depend on the x-y scanner, therefore a detector with a small aperture such as APD or a spectrometer can be used. Most of the earlier versions are descanned systems. A nondescanned system has its detector placed before the x-y scanners. The image of the signal on the detector depends on the position of the x-y scanner. Therefore, a large detector is commonly required in nondescanned system, which is more efficient than descanned system. It was found that the signal collection efficiency in a nondescanned system is about one or two orders higher than a descanned system.[50] Therefore, a nondescanned system is more suitable for *in vivo* applications.

MPM system. The first working version of MPM was adapted from a laser scanning confocal microscope.[1] Since then a number of MPM systems have been proposed but the main components remain similar. Young *et al.*[51] provided a pragmatic guide to build a customized MPM system. Lefort provided a detailed review of laser source for MPM system.[52] Zinter *et al.*[53] and Stoltzfus *et al.*[54] provided techniques for optimizing collection efficiency of MPM systems, respectively. A number of commercial MPM systems are currently available that are pushing this technology into different biomedical research fronts.[55]

CARS system. The first CARS microscope was proposed by Duncan *et al.* in 1982,[56] which relied on a noncollinear pump and Stokes beams originating from visible pulsed lasers. It has been substantially improved over the years after its initial discovery.[57] Both picosecond and femtosecond lasers have replaced previous pulsed lasers.[58,59] Recently, Xie and his colleagues developed a novel CARS microscopy that has high spatial resolution and imaging speeds, which has been widely used in biology, life sciences and medicine.[28,30,57] As shown in Sec. 1.2, one limitation of CARS is the nonresonant background (NRB), which restricts the spectral accuracy, systematic sensitivity and imaging contrast. In order to increase CARS contrast, a number of techniques have been proposed to suppress the NRB noise. One method is called E-CARS, in which the signal is detected in the epi-detection. CARS is a four-wave mixing process and the signal is usually in the forward direction. However, for highly scattered media such as skin, the forward CARS signal can be scattered back and collected in the epi-direction.[60,61] Another technique is called P-CARS for polarization-sensitive CARS detection. This method originates from different polarization properties of the resonant and nonresonant signals.[62–64] A third method is called T-CARS for time-resolved CARS detection. This technique utilizes an ultrashort pulsed laser as excitation, so that the resonant and nonresonant contributions are isolated in the time domain.[65,66] Usually, CARS is generated by two synchronized pulsed lasers. In order to simplify the laser system, a high-power picosecond oscillator with highly doped fibers for broadband Stokes generation has been proposed.[67] Photonic crystal fibers (PCFs) and a single femtosecond (fs) oscillator have also been adopted successfully.[68,69] When this method is applied by optimally chirped pulses, it creates a functioning multimodal CARS microscope that allows for optimal CARS performance while in the meantime recording TPF and SHG signals.[70] Picosecond pulse CARS system has higher

spectral resolution and favorable signal-to-background ratio using epi-detection geometry, polarization-sensitive detection and time-resolved CARS detection.[60]

Combined MPM and CARS system. Both MPM and CARS were developed based on the configuration of confocal microscopy. They share similar system configurations, as shown in Fig. 2, but with different laser sources and filtering optics. Therefore, both MPM and CARS can be combined into a single multimodal system.[37,71] Such a system has been used for imaging of normal skin, diseased skin and cancerous skin *in vivo*.[37,72–75]

2.2. *System characterization*

Resolution. The resolution of a MPM or CARS system is a very important parameter, which determines the optical sectioning capabilities of the system. Both the lateral and axial resolution can be predicted theoretically, which depends on the numerical aperture of the objective and the excitation wavelength.[76] However, because tissue scattering to the excitation light blurs focusing, the resolution is poorer than the theoretical prediction. The axial resolution of an MPM or CARS system is usually determined experimentally by measuring the signal of a thin layer of material or fluorescent beads.[57,77] For most biological applications of MPM or CARS systems, the lateral resolution is around 0.5 μm, and axial resolution is 1–5 μm. Over the years, there are a number of techniques proposed for super-resolution microscopy,[78] but it seems they are hard to be applied to *in vivo* human skin.

Field of view. The field of view (FOV) determines the area that can be imaged by MPM or CARS. Generally speaking, large FOV is very beneficial for many *in vivo* applications. It is determined by the focal length of the objective (magnification) and the scanning angle at the back aperture of the objective. Large FOVs (> mm) require low-magnification objective which has low-light collection efficiency. There are a number of methods proposed for improving the FOV of MPM and CARS systems. For example, McMullen *et al.*[79,80] proposed a ring detector to increase the collection efficiency in large FOV imaging. Tsai *et al.*[81] proposed a method that replaces singlet with compound scan lenses to minimize aberrations for ultra-large FOV imaging. Stirman *et al.*[82] and Grewe *et al.*[83] proposed respectively a method for wide FOV brain imaging. However, none of these techniques are easily applicable for the highly scattering skin tissue. Generally, the FOV for skin imaging is 500 μm × 500 μm. Balu *et al.*[84,85] reported an MPM system for skin imaging with a FOV of 800 μm × 800 μm and lateral resolution of 0.5 μm by optimizing the optics. Recently, they reported a fast, large area multiphoton exoscope (FLAME) for *in vivo* skin research which could provide high resolution depth-resolved images up to centimeter scale FOV.[86,87]

Imaging Speed. Imaging speed is one of the most important parameters for an *in vivo* MPM and CARS system. Imaging at fast frame rates is crucial to reduce image blurring due to patient motion and to provide practically short clinical measurement times. Earlier versions of MPM and CARS systems were converted from confocal microscopes and using photon counting detection method with slow imaging speed, which hampered their application for *in vivo* studies. Over the years, there are a number of techniques proposed for improving imaging speed, such as polygonal mirror scanners,[88] galvanometer scanners,[89] line scanners,[90] acoustic optical deflectors,[91] micro-lens-array-based scanners,[92–97] and *xy* resonant scanners.[98–100] Systems with polygonal mirror scanners and galvanometer scanners can achieve a frame rate up to 11 frames per second (fps).[88] Systems with line scanners can achieve a frame rate up to 30 fps, but the axial resolution is highly compromised, particularly for skin tissue.[90] Multifocal MPM system can achieve a frame rate from a few fps up to 600 fps. However, this type of instrument is usually in a descanned configuration, which is limited to exogenous fluorophores or low scattering medium. Recently, we have built the first video-rate multimodal MPM imaging systems based on raster resonant scanning and analog electronics detection for *in vivo* skin imaging at a frame rate up to 27 fps without the use of exogenous contrast agents.[100,101] Using this system, *in vivo* SHG and TPF images and videos could be acquired from the skin surface down to the reticular dermis.

Imaging Depth. The imaging depth of the conventional nondescanned and descanned MPM and CARS system is still limited, usually up to the top 100–200 μm. A number of techniques were proposed for deep tissue imaging, but none of them were seen for *in vivo* deep skin imaging. For example, Combs *et al.*[102–104] proposed a system using a parabolic light reflector to implement total emission

detection (TED) in both the transmission or reflection mode, which improved the signal-to-noise ratio by 10 fold. Engelbrecht *et al.*[105] proposed a supplementary fiber optic light collection system surrounding the objective for enhanced fluorescence imaging, which improved the signal gain by fourfold. Crosignani *et al.*[106–109] proposed a method for deep tissue imaging using a wide area detector, which was capable of imaging up to a few millimeters. McMullen *et al.*[79,80] proposed a circumferential ring detector based on fiber optics to enhance collection efficiency in large field-of-view multiphoton microscopy, which could increase the amount of collected signal by 20 fold. Singh *et al.*[110] compared the performance of a number of objective lenses and provided a framework for choosing objectives for multiphoton microscopy in turbid samples. Vucinic *et al.*[111] proposed a number of hybrid reflecting objectives for deep fluorescence imaging in turbid media. All these designs reported thus far are limited to exogenous fluorophores, biological phantoms or low-scattering biological tissues. It would be interesting to explore these techniques for *in vivo* deep skin imaging by collecting the emission signals as much as possible.

3. Evaluation of Normal Skin by MPM and CARS Imaging

Ex vivo studies of skin have been conducted to find the origin of the signals. Pena *et al.*[112] measured a histological section of human skin by MPM system using 860 nm excitation. It was found that epidermis had strong TPF without SHG, whereas dermis had strong SHG with intermediate TPF signals. The TPF signal of epidermis was mainly attributed to keratin, and the intermediate TPF signal in dermis was attributed to elastin. Collagen had measurable TPF signals only under excitation wavelength below 800 nm.[113] Chen *et al.*[39] systemically studied the spectral properties of *ex vivo* human skin using a tuneable femtosecond laser between 790 nm and 830 nm and similar results were obtained. The optimal excitation wavelength for SHG of dermal collagen was found to be 800 nm, similar to the results of extracted collagen samples.[114] In a backward imaging mode for a bulk tissue, both the TPF and SHG signal of *ex vivo* human skin dermis decreased monotonically with skin depth.[115]

Believe it or not, the first application of MPM in skin was an *in vivo* study.[21–23] The features of TPF and SHG for *in vivo* human skin are similar to those of *ex vivo* bulk tissue, but the quality of the *in vivo* images was not as good as those in the *ex vivo* studies, probably due to movement in the measurement. After the reported video-rate MPM system based on resonant scanners, the imaging quality of *in vivo* skin images is substantially improved.[100] An image stack of human skin *in vivo* using the video-rate MPM system is shown in Fig. 3.[100] It was an *in vivo* dorsal forearm skin under 740 nm excitation (80 MHz, 150 fs, FOV 200 μm $\times$ 200 μm). No TPF was observed for the cell nuclei. Cellular cytoplasm showed strong TPF probably due to NADH. Cell size decreased with the depth, from around 15–20 μm in diameter at depth about 25–30 μm to 8–10 μm in diameter at depth about 40–50 μm. The basal cell layer at the top of the papillary dermis also showed higher TPF, probably due to melanin fluorescence. The two-photon imaging of dermis was different from other skin layers, with the connective structures from TPF of elastin fibers and SHG of collagen fibers. Similar to *ex vivo* studies, *in vivo* measurement confirmed that epidermis had no SHG signal.

CARS was mainly used to study lipid and protein distribution in skin. The symmetric stretch vibration of lipids at 2845 cm^{-1} and asymmetric stretch at 2884 cm^{-1} were usually used for imaging as these are the strongest peaks of lipid, but other peaks could also be used in CARS imaging by properly choosing the pump and probe conditions.[30] Evans *et al.*[30,36] first reported a study of mouse ear tissue *in vivo*, in which bright polygonal patterns were found in the stratum corneum at the skin surface, due to lipids, ceramides and cholesterol. Sebaceous glands were usually seen at 20–40 μm from the skin surface, where they are packed in tiny, micrometer sized sebum reservoirs that have CH_2-rich triglycerides and wax esters. The authors in Ref. 116 also reported a longitudinal three-dimensional *in vivo* imaging of sebaceous glands in response to cryotherapy. CARS imaging of normal human skin was also reported, where the distribution of lipid and water in different skin layers were measured.[37,72] Combined MPM and CARS imaging of normal skin were also studied, where complementary information from different skin layers were identified.[37,71,72,75]

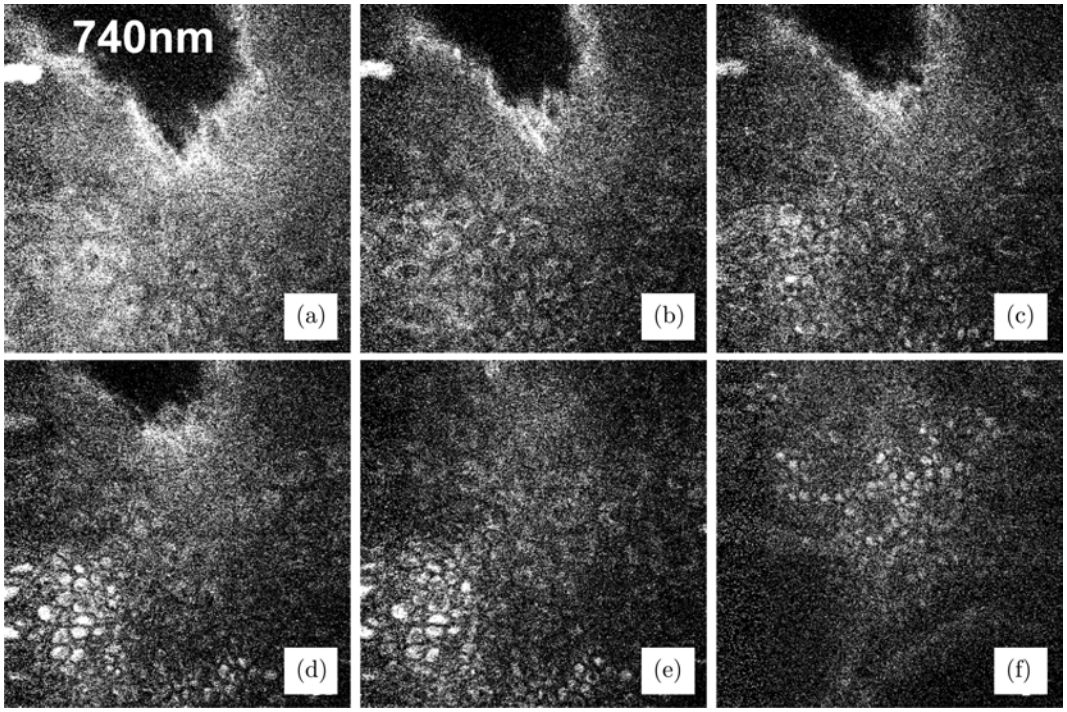

Fig. 3. TPF images of *in vivo* human dorsal forearm skin of a 25-year old Asian female increasing in depth from (a) near the surface to (f) near the dermal/epidermal boundary (Adapted from Lee *et al.*[100] with permission).

4. MPM and CARS for Skin Cancer and Skin Disease Diagnosis

Skin cancer is a very common malignancy, including melanoma, basal cell carcinoma (BCC) and squamous cell carcinoma (SCC). Both MPM and CARS have been explored in skin cancer and skin disease diagnosis. The major characteristics of normal skin and skin cancers are summarized in Table 2.

4.1. *BCC*

Lin *et al.*[117] first reported the studies of nodular BCC histological slices at 760 nm excitation using *ex vivo* MPM system. It was found that nodular BCC tumor cells have low two-photon fluorescence and large nonfluorescent nuclei. The SHG signals from cancer stroma decreased, indicating a disruption or deficiency of the triple-helical collagen fibers.[117] Later on, Paoli *et al.*[118] reported the MPM properties of *ex vivo* bulk tissues of nonmelanoma skin cancers and the surrounding normal skin at excitation of 780 nm. The morphologic features of all the perilesional normal skin agreed well with those of normal skin.[19,22,23] Cicchi *et al.*[119] and De Giorgi *et al.*[120] reported the diagnosis of BCC *ex vivo* using MPM and FLIM. It was found that all types of BCC lesions showed a blue-shift in fluorescence emission and a higher fluorescence lifetime than normal skin. Seidenari *et al.*[121–123] studied BCC and melanoma *ex vivo* by MPM and FLIM and proposed nine descriptors for BCC discrimination. Patalay *et al.*[124] reported BCC *ex vivo* using multispectral FLIM imaging and an area under receiver operating characteristic curve (ROC) as high as 0.83 was achieved. Similar to what was found by Cicchi *et al.*[119] cells in BCC were found to have significant increases in fluorescence lifetimes. Manfredini *et al.*[125] reported the comparison of MPM and reflectance confocal microscopy (RCM) imaging of BCC lesions using two independent MPM and RCM systems. Very recently, Balu *et al.*[126] reported the first *in vivo* study of BCC using a commercial MPM system, which revealed a number of features that were similar to those identified in *ex vivo* studies and confirmed the potential of MPM for *in vivo* BCC diagnosis and management. Heuke *et al.*[74] reported the detection and discrimination of BCC using multimodal imaging, and found that BCC lesion lacked SHG signal, and had weaker CARS signal. Furthermore, Legesse *et al.*[127] proposed the texture analysis for BCC classification based on CARS microscopic images.

Table 2. MPM and CARS features of normal skin, BCC, SCC and malignant melanoma.

Normal skin/ skin cancer	Major features
Normal skin	Epidermis: • Strong TPF due to keratin, no SHG • Cytoplasm has strong TPF due to NADH (excitation 740 nm) • Cell nucleus has no TPF and no SHG • Cell membranes show strong CARS signal Dermis: • Strong SHG due to collagen type 1 • Intermediate TPF due to elastin • Collagen has measurable TPF under < 800 nm excitation
Basal cell carcinoma	• Tumor cell has low TPF (760 nm excitation) • Large nucleus without TPF and SHG • Stroma has decreased TPF • Lack of SHG in dermis • Weaker CARS signal
Squamous cell carcinoma	• Larger nucleus without TPF and SHG • Higher nucleus-cytoplasm ratio • Higher intercellular distance • Lower cell density (nest has higher cell density) • Higher CARS signal
Malignant melanoma	• No distinctive skin layers • Oval, bright, homogenous and fluorescent melanocyte • Higher intercellular distance • Poorly defined cell borders • Irregularly shaped cells and pheomorphic cells • Long and highly fluorescent dendritic cells

4.2. *SCC*

The first *ex vivo* study of SCC was reported by Pauli *et al.*[118] where the main features of SCC *in situ* were summarized, such as thicker stratum corneum and irregular distributed cells within the stratum granulosum, stratum spinosum and stratum basal layers. There was no further report until very recently, Klemp *et al.*[128] studied six actinic keratosis (AK) (precursor of SCC) and six SCC patients *in vivo* using a commercial MPM system (MPTflex, JenLab GmbH, Jena, Germany). Significant differences were identified between AK, SCC and healthy skin. Both AK and SCC have larger nucleus diameters in stratum granulosum and stratum spinosum layer, higher nucleus-cytoplasm ratio, higher intercellular distance and lower cell density. SCC has much larger intercellular distance and lower cell density, which was also consistent with the findings by CARS imaging.[73] Different from BCC, SCC tissue showed higher CARS signal than the surrounding tissue.[74]

4.3. *Melanoma*

Application of TPF and SHG for malignant melanoma diagnosis was first reported by Dimitrow *et al.*[45,129] Six features were identified for differentiating melanoma from normal skin and benign skin lesions, including: Intercellular distance, degree of architectural disarray, cell border definition, and numbers of pleomorphic cells, ascending melanocytes and dendritic cells. It was found that the melanoma lesions had no distinctive skin layers. The melanocytes were oval, bright, homogenous and highly fluorescent. Large intercellular distances, poorly defined cell borders, irregularly shaped cells and polymorphic cells were usually observed. Long and highly fluorescent dendritic cells were also seen in malignant melanoma. While for benign melanocytic nevi, the keratinocytes were evenly distributed. Nevus cell nests were found with well-defined cell borders. Dendritic cells were rarely seen in benign melanocytic nevi. Remarkable differences were also found in lifetime imaging.[45] It was found that normal skin and pigmented nevi had single fluorescence peaks around 450 nm, while melanoma had a mild fluorescence peak around 470 nm and a second peak close to 550 nm. The 550 nm peak was assigned to melanin for malignant melanoma, consistent with the findings of Hoffman *et al.*[130] Another study also demonstrated that time-resolved fluorescence imaging was effective in discriminating healthy skin from malignant melanoma,[120] though it is limited to the number of cases. Balu *et al.*[131] reported melanoma diagnosis *in vivo* using a commercial MPM system. They proposed a three-parameter algorithm including fluorescence uniformity, second harmonic density and the density of melanocytic dendrites in the stratum spinosum and granulosum layers, which was found to be effective to classify melanoma lesions. Recently, Wang *et al.*[132] reported CARS imaging of pheomelanin *in vivo* in red-haired mouse. Till date, CARS imaging of melanoma has not been reported.

4.4. *Skin diseases*

Besides the applications of MPM and/or CARS system in normal skin studies and skin cancer diagnosis, it has also been used to evaluate a number of skin conditions, such as benign pigmented skin lesions,[133,134] scar tissue,[135–140] localized scleroderma,[141] atopic dermatitis (AD),[142] skin

stem cells[143,144] and psoriatic lesions.[145] It has also been used to study skin aging and photoaging,[146–155] cutaneous drug delivery,[156–167] light-tissue interactions,[168–171] wound healing process[172–176] and human skin immune responses.[177–186] However, most of these studies are still limited to either within the *ex vivo* applications or small number of cases. Numerous opportunities remain to be explored for *in vivo* and large-scale applications.

5. MPM for Imaging-Guided Two-Photon Photothermolysis

Till date, most of the studies of MPM in skin science are for noninvasive skin imaging and diagnosis. A number of studies addressed the laser safety of femto-second laser for imaging purpose.[187–197] We are the first group who has initiated the systematic study of utilizing the effect of multi-photon absorption for skin treatment.[198] We disclosed a technique for spatially-selective targeted photothermolysis based on two-photon absorption in 2014.[198] The treatment effect happens only within the focal volume and thus prevents damage of the surrounding tissues. Another beauty of the technique is that the treatment is guided through imaging, which provides real-time feedback to the operator. We subsequently refined this technique with the aim of developing *in vivo* applications.[199]

To demonstrate the concept, the two-photon absorption-based photothermolysis and the conventional photothermolysis are illustratively shown in Fig. 4(a). For conventional photothermolysis, both the target and other structures in the surrounding tissue that absorb the light are altered when the laser beam passes through them on the way to reach the target because the absorption is not spatially selective. While for two-photon absorption-based photothermolysis, only the target is treated because the nonlinear two-photon absorption effect is spatially selective, which only occurs at the focal point that is aligned with the target. Note that the laser wavelength for two-photo photothermolysis is different from conventional photothermolysis for the same targeted chromophore and thus two-photon photothermolysis prevents the side effect when the laser beam passes through the surrounding tissue. An implementation of imaging-guided two-photo photothermolysis is illustratively shown in Fig. 4(b). The imaging path (shown in green color) is used to locate the treatment target through real-time imaging guidance and the treatment path (magenta color) is used to focus the femto-second laser beam for spatially selective two-photon photothermolysis. An example of the spatially selective two-photon photothermolysis is shown in Fig. 5. It shows the MPM images (SHG: Green; TPF: Red) before and after two-photon photothermolysis under different

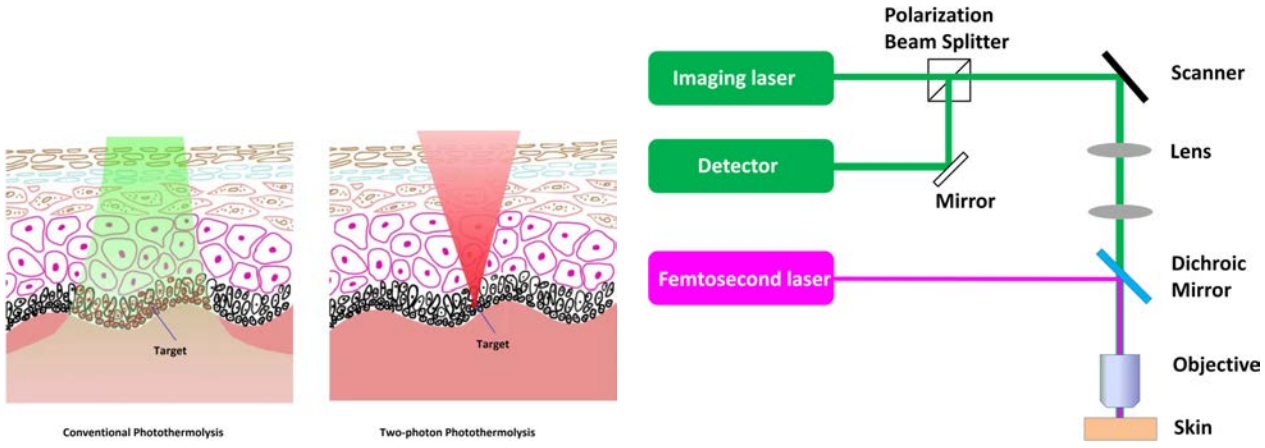

(a) (b)

Fig. 4. (a) Illustration of conventional photothermolysis and two-photon photothermolysis. Conventional photothermolysis is not spatially selective and the surrounding tissue is altered when the laser beam passes through. Two-photon photothermolysis is spatially selective and the surrounding tissue is unaltered when the laser beam passes through because the laser wavelength is different from the conventional photothermolysis for the same targeted chromophore. (b) Schematic diagram of an implementation of imaging-guided two-photon photothermolysis. The imaging path (shown in green color) is used to locate the treatment target through real-time imaging guidance, and the treatment path (magenta color) is used to focus the femtosecond laser beam for two-photon photothermolysis. (Adapted from Huang *et al.*[199] with permission).

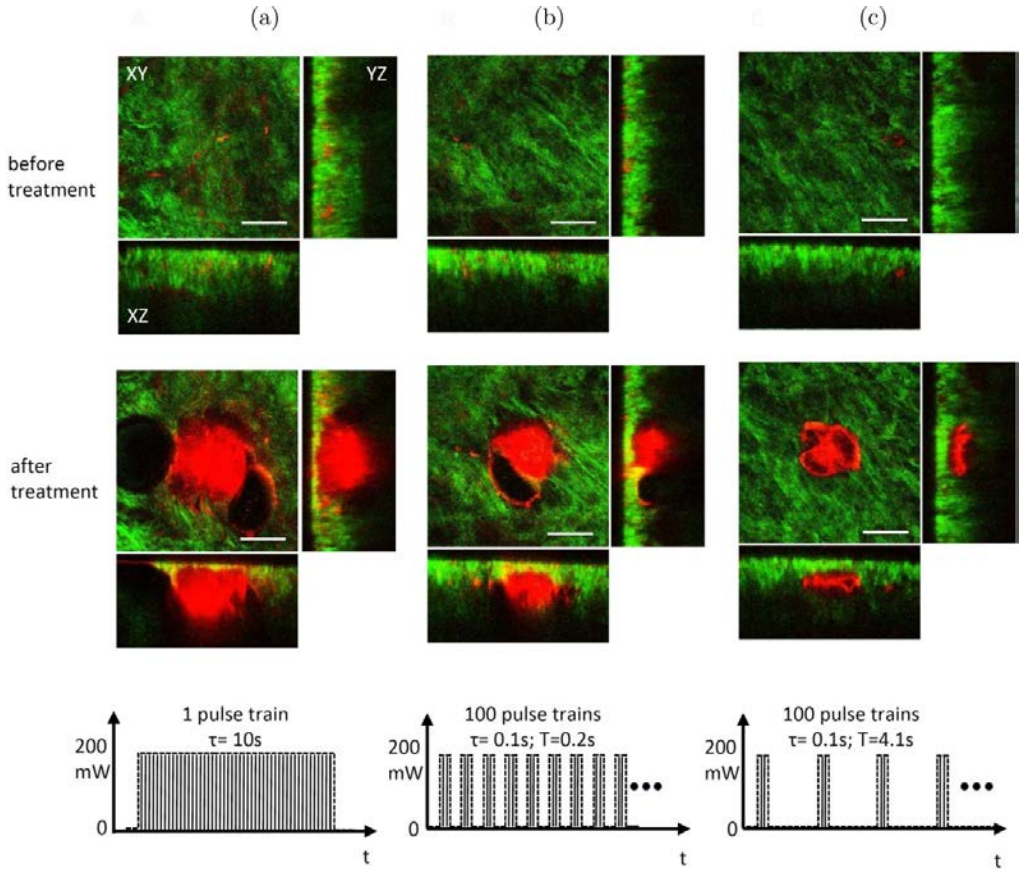

Fig. 5. Spatially-selective photothermolysis based on two-photon absorption under different laser treatment strategies: (a) Treatment of 10 s with a single session of femtosecond pulses (80 MHz, 150 fs), (b) treatment of 10 s with 100 sessions of femtosecond pulses with each session of 0.1 s and an interval between sessions of 0.2 s, (c) treatment of 10 s with 100 sessions with each session of 0.1 s and an interval between sessions of 4.1 s. The targeted area is 50 μm × 50 μm, located in the center of the XY image and 40 μm beneath the tissue surface. Note that the treatment effect can be well controlled by different strategies and the surrounding layers of the targeted area remain intact after treatment. Wavelength: 800 nm. Laser intensity: 200 mW. Scale bars: 50 μm. (Adapted from Huang *et al.*[199] with permission).

strategies. The targeted area is 50 μm × 50 μm, located in the center of the XY image and 40 μm beneath the tissue surface. Note that the treatment effect can be well controlled by different strategies and the surrounding layers of the targeted area remain intact after treatment. Recently, using a mouse ear model, we have successfully demonstrated this two-photon absorption based, spatially selective photothermolysis technique to be an effective approach for noninvasive precise microsurgery of vascular disease on a per vessel/per lesion basis.[200] This is a precise "see and treat" microsurgery method, not only works for skin, but also holds particular promise for treating disease in complex organs such as the eye (noninvasively) or brain, where high spatial selectivity is critical for preventing collateral effects on vision or central nervous system function.

6. Summary

In summary, we present the basics, development and applications of MPM and CARS for *in vivo* skin studies. MPM and CARS have numerous advantages over traditional single-photon excitation fluorescence and confocal microscopy. Since the inception of multi-photon fluorescence and CARS microscopy, development of MPM and CARS has been substantial in every aspect, including imaging speed, FOV and imaging depth. A lot of opportunities remain to be developed to push this technology from lab to point-of-care clinical applications.[75] Combination of MPM and CARS with other modalities such as optical coherence tomography (OCT)[201,202] or Raman spectroscopy,[203] will provide further information for skin evaluation. Instrumentation-wise, with technical advances in

lasers and scanning technology, particularly with the endoscopic multiphoton development,[204–209] we expect a portable, compact, miniaturized MPM and CARS system; with video-rate imaging speed and deep imaging capabilities which will be within reach for clinical skin applications in the near future.

Conflict of Interest

The authors declare no conflicts of interest.

Acknowledgments

This work is supported partially by the Canadian Institutes of Health Research and the Canadian Dermatology Foundation. Dr. Yimei Huang is greatly acknowledged for providing some of the figures.

References

1. W. Denk, J. H. Strickler, W. W. Webb, "Two photon laser scanning fluorescence microscopy," *Science* **248**, 73–76 (1990).
2. R. Williams, D. Piston, W. Webb, "Two-photon molecular excitation provides intrinsic 3-dimensional resolution for laser-based microscopy and microphotochemistry," *FASEB J.* **8**, 804–813 (1994).
3. C. Xu, W. W. Webb, "Measurement of two-photon excitation cross sections of molecular fluorophores with data from 690 to 1050 nm," *J. Opt. Soc. Am. B* **13**, 481–491 (1996).
4. P. T. C. So, C. Y. Dong, B. R. Masters, K. M. Berland, "Two-photon excitation fluorescence microscopy," *Annu. Rev. Biomed. Eng.* **2**, 399–429 (2000).
5. P. Schwille, U. Haupts, S. Maiti, W. W. Webb, "Molecular dynamics in living cells observed by fluorescence correlation spectroscopy with one- and two-photon excitation," *Biophys. J.* **77**, 2251–2265 (1999).
6. M. Rubart, "Two-photon microscopy of cells and tissue," *Circ. Res.* **95**, 1154–1166 (2004).
7. D. W. Piston, "Imaging living cells and tissues by two-photon excitation microscopy," *Trends Cell Biol.* **9**, 66–69 (1999).
8. J. Sawinski, W. Denk, "Miniature random-access fiber scanner for *in vivo* multiphoton imaging," *J. Appl. Phys.* **102**, 034701 (2007).
9. K. Svoboda, R. Yasuda, "Principles of two-photon excitation microscopy and its applications to neuroscience," *Neuron* **50**, 823–839 (2006).
10. W. Denk, K. R. Delaney, A. Gelperin, D. Kleinfeld, B. W. Strowbridge, D. W. Tank, R. Yuste, "Anatomical and functional imaging of neurons using 2-photon laser scanning microscopy," *J. Neurosci. Meth.* **54**, 151–162 (1994).
11. C. Stosiek, O. Garaschuk, K. Holthoff, A. Konnerth, "*In vivo* two-photon calcium imaging of neuronal networks," *Proc. Natl. Acad. Sci. USA* **100**, 7319–7324 (2003).
12. M. Oheim, E. Beaurepaire, E. Chaigneau, J. Mertz, S. Charpak, "Two-photon microscopy in brain tissue: parameters influencing the imaging depth," *J. Neurosci. Meth.* **111**, 29–37 (2001).
13. R. Nitsch, E. E. Pohl, A. Smorodchenko, C. Infante-Duarte, O. Aktas, F. Zipp, "Direct impact of T cells on neurons revealed by two-photon microscopy in living brian tissue," *J. Neurosci.* **24**, 2458–2464 (2004).
14. G. E. Stutzmann, F. M. LaFerla, I. Parker, "Ca2+ signaling in mouse cortical neurons studied by two-photon imaging and photoreleased inositol triphosphate," *J. Neurosci.* **23**, 758–765 (2003).
15. N. Ji, J. Freeman, S. L. Smith, "Technologies for imaging neural activity in large volumes," *Nat. Neurosci.* **19**, 1154–1164 (2016).
16. J. M. Squirrell, D. L. Wokosin, J. G. White, B. D. Bavister, "Long-term two-photon fluorescence imaging of mammalian embryos without compromising viability," *Nat. Biotechnol.* **17**, 763–767 (1999).
17. R. Cicchi, D. Kapsokalyvas, F. S. Pavone, "Clinical nonlinear laser imaging of human Skin: A review," *Biomed. Res. Int.* **2014**, 14 (2014).
18. E. Yew, C. Rowlands, P. T. C. So, "Application of multiphoton microscopy in dermatological studies: A mini-review," *J. Innov. Opt. Health Sci.* **7**, 1330010 (2014).
19. K. Konig, I. Riemann, "High-resolution multiphoton tomography of human skin with subcellular spatial resolution and picosecond time resolution," *J. Biomed. Opt.* **8**, 432–439 (2003).
20. B. R. Masters, P. T. C. So, "Multi-photon excitation microscopy and confocal microscopy imaging of *in vivo* human skin: A comparison," *Microsc. Microanal.* **5**, 282–289 (1999).
21. B. R. Masters, P. T. C. So, "Confocal microscopy and multi-photon excitation microscopy of human skin *in vivo*," *Opt. Exp.* **8**, 2–10 (2000).
22. B. R. Masters, P. T. C. So, E. Gratton, "Multiphoton excitation fluorescence microscopy and spectroscopy of *in vivo* human skin," *Biophys. J.* **72**, 2405–2412 (1997).
23. B. R. Masters, P. T. C. So, E. Gratton, "Optical biopsy of *in vivo* human skin: Multi-photon excitation microscopy," *Lasers Med. Sci.* **13**, 196–203 (1998).

24. J. Condeelis, J. E. Segall, "Intravital imaging of cell movement in tumours," *Nat. Rev. Cancer* **3**, 921–930 (2003).
25. M. Lohela, Z. Werb, "Intravital imaging of stromal cell dynamics in tumors," *Curr. Opin. Gen. Dev.* **20**, 72–78 (2010).
26. M. J. Miller, S. H. Wei, M. D. Cahalan, I. Parker, "Autonomous T cell trafficking examined *in vivo* with intravital two-photon microscopy," *Proc. Natl. Acad. Sci.* **100**, 2604–2609 (2003).
27. T. Honda, A. Otsuka, K. Kabashima, "Novel insights into cutaneous immune systems revealed by *in vivo* imaging," *Allergol. Int.* **65**, 228–234 (2016).
28. J. X. Cheng, X. S. Xie, "Coherent anti-Storkes Raman scattering microscopy: Instrumentation, theory and applications," *J. Phys. Chem. B* **108**, 827–840 (2004).
29. C. Krafft, B. Dietzek, J. Popp, "Raman and CARS microspectroscopy of cells and tissues," *Analyst* **134**, 1046–1057 (2009).
30. C. L. Evans, X. S. Xie, "Coherent anti-Stokes Raman scattering microscopy: Chemical imaging for biology and medicine," *Annu. Rev. Anal. Chem.* **1**, 883–909 (2008).
31. X. Nan, J.-X. Cheng, X. S. Xie, "Vibrational imaging of lipid droplets in live fibroblast cells with coherent anti-Stokes Raman scattering microscopy," *J. Lipid Res.* **44**, 2202–2208 (2003).
32. J.-X. Cheng, L. D. Book, X. S. Xie, "Polarization coherent anti-Stokes Raman scattering microscopy," *Opt. Lett.* **26**, 1341–1343 (2001).
33. E. O. Potma, W. P. de Boeij, P. J. van Haastert, D. A. Wiersma, "Real-time visualization of intracellular hydrodynamics in single living cells," *Proc. Natl. Acad. Sci.* **98**, 1577–1582 (2001).
34. E. O. Potma, X. S. Xie, "Detection of single lipid bilayers with coherent anti-Stokes Raman scattering (CARS) microscopy," *J. Raman Spectrosc.* **34**, 642–650 (2003).
35. G. W. Wurpel, J. M. Schins, M. Müller, "Direct measurement of chain order in single phospholipid mono-and bilayers with multiplex CARS," *J. Phys. Chem. B* **108**, 3400–3403 (2004).
36. C. L. Evans, E. O. Potma, M. Puoris' haag, D. Côté, C. P. Lin, X. S. Xie, "Chemical imaging of tissue *in vivo* with video-rate coherent anti-Stokes Raman scattering microscopy," *Proc. Natl. Acad. Sci. USA* **102**, 16807–16812 (2005).
37. K. König, H. Breunig, R. Bückle, M. Kellner-Höfer, M. Weinigel, E. Büttner, W. Sterry, J. Lademann, "Optical skin biopsies by clinical CARS and multiphoton fluorescence/SHG tomography," *Laser Phys. Lett.* **8**, 465–468 (2011).
38. J. Chen, A. Lee, J. Zhao, H. Wang, H. Lui, D. I. McLean, H. Zeng, "Spectroscopic characterization and microscopic imaging of extracted and *in situ* cutaneous collagen and elastic tissue components under two-photon excitation," *Skin Res. Technol.* **15**, 418–426 (2009).
39. J. Chen, S. Zhuo, T. Luo, X. Jiang, J. Zhao, "Spectral characteristics of autofluorescence and second harmonic generation from *ex vivo* human skin induced by femtosecond laser and visible lasers," *Scanning* **28**, 319–326 (2006).
40. M. Shen, Y. Tian, S. P. Chong, J. Zhao, H. Zeng, S. Tang, "Quantifying the backscattering of second harmonic generation in tissues with confocal multiphoton microscopy," *J. Biomed. Opt.* **18**, 115003 (2013).
41. M. Shen, J. Zhao, H. Zeng, S. Tang, "Calibrating the measurement of wavelength-dependent second harmonic generation from biological tissues with a BaB(2)O(4) crystal," *J. Biomed. Opt.* **18**, 031109 (2013).
42. P. Stoller, K. M. Reiser, P. M. Celliers, A. M. Rubenchik, "Polarization-modulated second harmonic generation in collagen," *Biophys. J.* **82**, 3330–3342 (2002).
43. M. Strupler, A. M. Pena, M. Hernest, P. L. Tharaux, J. L. Martin, E. Beaurepaire, M. C. Schanne-klein, "Second harmonic imaging and scoring of collagen in fibrotic tissues," *Opt Exp.* **15**, 4054–4065 (2007).
44. S.-Y. Chen, H.-Y. Wu, C.-K. Sun, "*In vivo* harmonic generation biopsy of human skin," *J. Biomed. Opt.* **14**, 060505-060505-3 (2009).
45. E. Dimitrow, I. Riemann, J. Ehlers, M. J. Koehler, J. Norgauer, P. Elsner, K. Konig, M. Kaatz, "Spectral fluorescence lifetime detection and selective melanin imaging by multiphoton laser tomography for melanoma diagnosis," *Exp. Dermatol.* **18**, 509–515 (2009).
46. M. J. Koehler, A. Preller, P. Elsner, K. König, U. C. Hipler, M. Kaatz, "Non-invasive evaluation of dermal elastosis by *in vivo* multiphoton tomography with autofluorescence lifetime measurements," *Exp. Dermatol.* **21**, 48–51 (2012).
47. K. Konig, "Clinical multiphoton tomography," *J. Biophoton.* **1**, 13–23 (2008).
48. K. König, "Clinical *in vivo* multiphoton FLIM tomography," *Meth. Appl. Fluorescence* **8**, 034002 (2020).
49. F. Helmchen, W. Denk, "Deep tissue two-photon microscopy," *Nat. Meth.* **2**, 932–940 (2005).
50. Y. Le Grand, A. Leray, T. Guilbert, C. Odin, "Non-descanned versus descanned epifluorescence collection in two-photon microscopy: Experiments and Monte Carlo simulations," *Opt. Commun.* **281**, 5480–5486 (2008).

51. M. D. Young, J. J. Field, K. E. Sheetz, R. A. Bartels, J. Squier, "A pragmatic guide to multiphoton microscope design," *Adv. Opt. Photon.* **7**, 276–378 (2015).
52. C. Lefort, "A review of biomedical multiphoton microscopy and its laser sources," *J. Phys. D. Appl. Phys.* **50**, 423001 (2017).
53. J. P. Zinter, M. J. Levene, "Maximizing fluorescence collection efficiency in multiphoton microscopy," *Opt. Exp.* **19**, 15348–15362 (2011).
54. C. R. Stoltzfus, A. Rebane, "Optimizing ultrafast illumination for multiphoton-excited fluorescence imaging," *Biomed. Opt. Exp.* **7**, 1768–1782 (2016).
55. K. Koenig, "Hybrid multiphoton multimodal tomography of *in vivo* human skin," *IntraVital* **1**, 11–26 (2012).
56. M. D. Duncan, J. Reintjes, T. Manuccia, "Scanning coherent anti-Stokes Raman microscope," *Opt. Lett.* **7**, 350–352 (1982).
57. A. Zumbusch, G. R. Holtom, X. S. Xie, "Three-dimensional vibrational imaging by coherent anti-Stokes Raman scattering," *Phys. Rev. Lett.* **82**, 4142 (1999).
58. E. O. Potma, D. J. Jones, J.-X. Cheng, X. S. Xie, J. Ye, "High-sensitivity coherent anti-Stokes Raman scattering microscopy with two tightly synchronized picosecond lasers," *Opt. Lett.* **27**, 1168–1170 (2002).
59. M. Müller, J. M. Schins, "Imaging the thermodynamic state of lipid membranes with multiplex CARS microscopy," *J. Phys. Chem. B* **106**, 3715–3723 (2002).
60. J.-X. Cheng, A. Volkmer, L. D. Book, X. S. Xie, "An epi-detected coherent anti-Stokes Raman scattering (E-CARS) microscope with high spectral resolution and high sensitivity," *J. Phys. Chem. B* **105**, 1277–1280 (2001).
61. A. Volkmer, J.-X. Cheng, X. S. Xie, "Vibrational imaging with high sensitivity via epidetected coherent anti-Stokes Raman scattering microscopy," *Phys. Rev. Lett.* **87**, 023901 (2001).
62. S. Akhmanov, A. Bunkin, S. Ivanov, N. Koroteev, "Coherent ellipsometry of Raman scattering of light," *Sov. J. Exp. Theor. Phys. Lett.* **25**, 416 (1977).
63. J. L. Oudar, R. W. Smith, Y. Shen, "Polarization-sensitive coherent anti-Stokes Raman spectroscopy," *Appl. Phys. Lett.* **34**, 758–760 (1979).
64. R. Brakel, F. W. Schneider, "Polarization CARS spectroscopy," *Adv. Non-Linear Spectrosc.*, R. J. H. Clark and R. E. Hester, eds. Vol 15 (Wiley, New York, 1988), pp. 149–193.
65. A. Laubereau, W. Kaiser, "Vibrational dynamics of liquids and solids investigated by picosecond light pulses," *Rev. Mod. Phys.* **50**, 607 (1978).
66. F. M. Kamga, M. G. Sceats, "Pulse-sequenced coherent anti-Stokes Raman scattering spectroscopy: A method for suppression of the nonresonant background," *Opt. Lett.* **5**, 126 (1980).
67. G. I. Petrov, V. V. Yakovlev, "Enhancing red-shifted white-light continuum generation in optical fibers for applications in nonlinear Raman microscopy," *Opt. Exp.* **13**, 1299–1306 (2005).
68. H. N. Paulsen, K. M. Hilligse, J. Thøgersen, S. R. Keiding, J. J. Larsen, "Coherent anti-Stokes Raman scattering microscopy with a photonic crystal fiber based light source," *Opt. Lett.* **28**, 1123–1125 (2003).
69. E. R. Andresen, H. N. Paulsen, V. Birkedal, J. Thøgersen, S. R. Keiding, "Broadband multiplex coherent anti-Stokes Raman scattering microscopy employing photonic-crystal fibers," *J. Opt. Soc. Am. B* **22**, 1934–1938 (2005).
70. A. F. Pegoraro, A. Ridsdale, D. J. Moffatt, Y. Jia, J. P. Pezacki, A. Stolow, "Optimally chirped multimodal CARS microscopy based on a single Ti: sapphire oscillator," *Opt. Exp.* **17**, 2984–2996 (2009).
71. S. Heuke, N. Vogler, T. Meyer, D. Akimov, F. Kluschke, H. J. Röwert-Huber, J. Lademann, B. Dietzek, J. Popp, "Multimodal mapping of human skin," *Br. J. Dermatol.* **169**, 794–803 (2013).
72. H. G. Breunig, R. Bückle, M. Kellner-Höfer, M. Weinigel, J. Lademann, W. Sterry, K. König, "Combined *in vivo* multiphoton and CARS imaging of healthy and disease-affected human skin," *Microsc. Res. Tech.* **75**, 492–498 (2012).
73. M. Weinigel, H. Breunig, M. Kellner-Höfer, R. Bückle, M. Darvin, M. Klemp, J. Lademann, K. König, "*In vivo* histology: Optical biopsies with chemical contrast using clinical multiphoton/coherent anti-Stokes Raman scattering tomography," *Laser Phys. Lett.* **11**, 055601 (2014).
74. S. Heuke, N. Vogler, T. Meyer, D. Akimov, F. Kluschke, H.-J. Röwert-Huber, J. Lademann, B. Dietzek, J. Popp, "Detection and discrimination of non-melanoma skin cancer by multimodal imaging," *Healthcare* **1**, 64–83 (2013).
75. K. König, H. G. Breunig, A. Batista, A. Schindele, M. Zieger, M. Kaatz, "Translation of two-photon microscopy to the clinic: Multimodal multiphoton CARS tomography of *in vivo* human skin," *J. Biomed. Opt.* **25**, 014515 (2020).
76. W. R. Zipfel, R. M. Williams, W. W. Webb, "Nonlinear magic: Multiphoton microscopy in the biosciences," *Nat. Biotechnol.* **21**, 1369–1377 (2003).
77. M. Schrader, U. G. Hofmann, S. W. Hell, "Ultrathin fluorescent layers for monitoring the axial resolution in confocal and two-photon

fluorescence microscopy," *J. Microsc.* **191**, 135–140 (1997).
78. B. Huang, M. Bates, X. Zhuang, "Super resolution fluorescence microscopy," *Annu. Rev. Biochem.* **78**, 993 (2009).
79. J. McMullen, A. Kwan, R. Williams, W. Zipfel, "Enhancing collection efficiency in large field of view multiphoton microscopy," *J. Microsc.* **241**, 119–124 (2011).
80. J. D. McMullen, W. R. Zipfel, "A multiphoton objective design with incorporated beam splitter for enhanced fluorescence collection," *Opt. Exp.* **18**, 5390–5398 (2010).
81. P. S. Tsai, C. Mateo, J. J. Field, C. B. Schaffer, M. E. Anderson, D. Kleinfeld, "Ultra-large field-of-view two-photon microscopy," *Opt. Exp.* **23**, 13833–13847 (2015).
82. J. N. Stirman, I. T. Smith, M. W. Kudenov, S. L. Smith, "Wide field-of-view, multi-region, two-photon imaging of neuronal activity in the mammalian brain," *Nat. Biotechnol.* **34**, 857–862 (2016).
83. B. F. Grewe, F. F. Voigt, M. van't Hoff, F. Helmchen, "Fast two-layer two-photon imaging of neuronal cell populations using an electrically tunable lens," *Biomed. Opt. Exp.* **2**, 2035–2046 (2011).
84. M. Balu, H. Mikami, J. Hou, E. O. Potma, B. J. Tromberg, Large field of view multiphoton microscopy of human skin, *Proc. SPIE 9712, Multiphoton Microscopy in the Biomedical Sciences XVI*, Vol. 97121F (2016), doi: 10.1117/12.2216163.
85. M. Balu, H. Mikami, J. Hou, E. O. Potma, B. J. Tromberg, "Rapid mesoscale multiphoton microscopy of human skin," *Biomed. Opt. Exp.* **7**, 4375–4387 (2016).
86. A. Fast, A. Lal, A. F. Durkin, G. Lentsch, R. M. Harris, C. B. Zachary, A. K. Ganesan, M. Balu, "Fast, large area multiphoton exoscope (FLAME) for macroscopic imaging with microscopic resolution of human skin," *Sci. Rep.* **10**, 1–14 (2020).
87. J. R. Vicente, A. Durkin, K. Shrestha, M. Balu, "*In vivo* imaging with a fast large-area multiphoton exoscope (FLAME) captures the melanin distribution heterogeneity in human skin," *Sci. Rep.* **12**, 1–10 (2022).
88. K. H. Kim, C. Buehler, P. T. C. So, "High-speed, two-photon scanning microscope," *Appl. Opt.* **38**, 6004–6009 (1999).
89. S. W. Chu, T. M. Liu, C. K. Sun, C. Y. Lin, H. J. Tsai, "Real-time second harmonic-generation microscopy based on a 2-GHz repetition rate Ti:sapphire laser," *Opt. Exp.* **11**, 933–938 (2003).
90. G. Brakenhoff, J. Squier, T. Norris, A. C. Bliton, M. Wade, B. Athey, "Real-time two-photon confocal microscopy using a femtosecond, amplified Ti: sapphire system," *J. Microsc.* **181**, 253–259 (1996).
91. J. D. Lechleiter, D. T. Lin, I. Sieneart, "Multiphoton laser scanning microscopy using an acoustic optical deflector," *Biophys. J.* **83**, 2292–2299 (2002).
92. J. Bewersdorf, R. Pick, S. W. Hell, "Multifocal multiphoton microscopy," *Opt. Lett.* **23**, 655–657 (1998).
93. M. Kobayashi, K. Fujita, T. Kaneko, T. Takamatsu, O. Nakamura, S. Kawata, "Second-harmonic-generation microscope with a microlens array scanner," *Opt. Lett.* **27**, 1324–1326 (2002).
94. K. Fujita, O. Nakamura, T. Kaneko, M. Oyamada, T. Takamatsu, S. Kawata, "Confocal multipoint multiphoton excitation microscope with microlens and pinhole arrays," *Opt. Commun.* **174**, 7–12 (2000).
95. K. H. Kim, C. Buehler, K. Bahlmann, T. Ragan, W.-C. A. Lee, E. Nedivi, E. L. Heffer, S. Fantini, P. T. So, "Multifocal multiphoton microscopy based on multianode photomultiplier tubes," *Opt. Exp.* **15**, 11658–11678 (2007).
96. K. Bahlmann, P. T. So, M. Kirber, R. Reich, B. Kosicki, W. McGonagle, K. Bellve, "Multifocal multiphoton microscopy (MMM) at a frame rate beyond 600 Hz," *Opt. Exp.* **15**, 10991–10998 (2007).
97. J. W. Cha, E. Y. Yew, D. Kim, J. Subramanian, E. Nedivi, P. T. So, "Non-descanned multifocal multiphoton microscopy with a multianode photomultiplier tube," *AIP Adv.* **5**, 084802 (2015).
98. G. Y. Fan, H. Fujisaki, A. Miyawaki, R. K. Tsay, R. Y. Tisen, M. H. Ellisman, "Video-rate scanning two-photon excitation fluorescence microscopy and ratio imaging with cameleons," *Biophys. J.* **76**, 2412–2420 (1999).
99. A. Lee, H. Wang, Y. Yu, J. Zhao, S. Tang, H. Lui, D. I. McLean, H. Zeng, "New multimodal multiphoton imaging and spectroscopy apparatus for dermatology," *ECS Meet. Abs.* **MA2010-01**, 1059 (2010).
100. A. Lee, H. Wang, Y. Yu, S. Tang, J. Zhao, H. Lui, D. I. McLean, H. Zeng, "*In vivo* video rate multiphoton microscopy imaging of human skin," *Opt. Lett.* **36**, 2865–2867 (2011).
101. H. Wang, A. M. D. Lee, Z. Frehlick, H. Lui, D. I. McLean, S. Tang, H. Zeng, "Perfectly registered multiphoton and reflectance confocal video rate imaging of *in vivo* human skin," *J. Biophoton.* **6**, 305–309 (2013).
102. C. A. Combs, A. V. Smirnov, J. D. Riley, A. H. Gandjbakhche, J. R. Knutson, R. S. Balaban, "Optimization of multiphoton excitation microscopy by total emission detection using a parabolic light reflector," *J. Microsc.* **228**, 330–337 (2007).
103. C. A. Combs, A. Smirnov, D. Chess, D. B. McGavern, J. L. Schroeder, J. Riley, S. S. Kang, LUGAR-HAMMER M., A. Gandjbakhche, J. R.

Knutson, "Optimizing multiphoton fluorescence microscopy light collection from living tissue by noncontact total emission detection (epiTED)," *J. Microsc.* **241**, 153–161 (2011).
104. C. A. Combs, A. Smirnov, B. Glancy, N. S. Karamzadeh, A. H. Gandjbakhche, G. Redford, K. Kilborn, J. R. Knutson, R. S. Balaban, "Compact non-contact total emission detection for *in vivo* multiphoton excitation microscopy," *J. Microsc.* **253**, 83–92 (2014).
105. C. J. Engelbrecht, W. Göbel, F. Helmchen, "Enhanced fluorescence signal in nonlinear microscopy through supplementary fiber-optic light collection," *Opt. Exp.* **17**, 6421–6435 (2009).
106. V. Crosignani, A. S. Dvornikov, E. Gratton, "Enhancement of imaging depth in turbid media using a wide area detector," *J. Biophoton.* **4**, 592–599 (2011).
107. V. Crosignani, S. Jahid, A. Dvornikov, E. Gratton, "Deep tissue imaging by enhanced photon collection," *J. Innov. Opt. Health Sci.* **7**, 1450034 (2014).
108. V. Crosignani, A. Dvornikov, J. S. Aguilar, C. Stringari, R. Edwards, W. W. Mantulin, E. Gratton, "Deep tissue fluorescence imaging and *in vivo* biological applications," *J. Biomed. Opt.* **17**, 116023 (2012).
109. V. Crosignani, S. Jahid, A. S. Dvornikov, E. Gratton, "A deep tissue fluorescence imaging system with enhanced SHG detection capabilities," *Microsc. Res. Tech.* **77**, 368–373 (2014).
110. A. Singh, J. D. McMullen, E. A. Doris, W. R. Zipfel, "Comparison of objective lenses for multiphoton microscopy in turbid samples," *Biomed. Opt. Exp.* **6**, 3113–3127 (2015).
111. D. Vucinic, T. M. BartolJr, T. J. Sejnowski, "Hybrid reflecting objectives for functional multiphoton microscopy in turbid media," *Opt. Lett.* **31**, 2447–2449 (2006).
112. A. M. Pena, M. Strupler, T. Boulesteix, M. C. Schanne-Klein, "Spectroscopic analysis of keratin endogenous signal for skin multiphoton microscopy," *Opt. Exp.* **13**, 6268–6274 (2005).
113. A. Zoumi, A. Yeh, B. J. Tromberg, "Imaging cells and extracellular matrix *in vivo* by using second-harmonic generation and two photon excited fluorescence," *Proc. Natl. Acad. Sci. USA* **99**, 11014–11019 (2002).
114. J. Chen, A. Lee, J. Zhao, H. Wang, H. Lui, D. I. McLean, H. Zeng, "Spectroscopic characterization and microscopic imaging of extracted and *in situ* cutaneous collagen and elastin tissue components under two-photon excitation," *Skin Res. Technol.* **15**, 418–426 (2009).
115. S. Zhuo, J. Chen, T. Luo, D. Zou, J. Zhao, "Multimode nonlinear optical imaging of the dermis in *ex vivo* human skin based on the combinatin of multichannel mode and lambda mode," *Opt. Exp.* **14**, 7810–7820 (2006).
116. Y. Jung, J. Tam, H. R. Jalian, R. R. Anderson, C. L. Evans, "Longitudinal, 3D *in vivo* imaging of sebaceous glands by coherent anti-Stokes Raman scattering microscopy: Normal function and response to cryotherapy," *J. Invest. Dermatol.* **135**, 39–44 (2015).
117. S. J. Lin, S. H. Jee, J. K. C., R. J. Wu, W. C. Lin, J. S. Chen, Y. H. Liao, C. J. Hsu, T. F. Tsai, Y. F. Chen, C. Y. Dong, "Discrimination of basal cell carcinoma from normal dermal stroma by quantitative multiphoton imaging," *Opt. Lett.* **31**, 2756–2758 (2006).
118. J. Paoli, M. Smedh, A. M. Wennberg, M. B. Ericson, "Multiphoton laser scanning microscopy on non-melanoma skin cancer: Morphologic features for future non-invasive diagnostics," *J. Invest. Dermatol.* **128**, 1248–1255 (2008).
119. R. Cicchi, D. Massi, S. Sestini, P. Carli, V. De Giorgi, T. Lotti, F. Pavone, "Multidimensional non-linear laser imaging of Basal Cell Carcinoma," *Opt. Exp.* **15**, 10135–10148 (2007).
120. V. De Giorgi, D. Massi, S. Sestini, R. Cicchi, F. Pavone, T. Lotti, "Combined non-linear laser imaging (two-photon excitation fluorescence microscopy, fluorescence lifetime imaging microscopy, multispectral multiphoton microscopy) in cutaneous tumours: First experiences," *J. Eur. Acad. Dermatol. Venereol.* **23**, 314–316 (2009).
121. S. Seidenari, F. Arginelli, S. Bassoli, J. Cautela, A. M. Cesinaro, M. Guanti, D. Guardoli, C. Magnoni, M. Manfredini, G. Ponti, "Diagnosis of BCC by multiphoton laser tomography," *Skin Res. Technol.* **19**, e297–e304 (2013).
122. S. Seidenari, F. Arginelli, C. Dunsby, P. French, K. König, C. Magnoni, M. Manfredini, C. Talbot, G. Ponti, "Multiphoton laser tomography and fluorescence lifetime imaging of basal cell carcinoma: Morphologic features for non-invasive diagnostics," *Exp. Dermatol.* **21**, 831–836 (2012).
123. S. Seidenari, F. Arginelli, C. Dunsby, P. M. French, K. König, C. Magnoni, C. Talbot, G. Ponti, "Multiphoton laser tomography and fluorescence lifetime imaging of melanoma: Morphologic features and quantitative data for sensitive and specific non-invasive diagnostics," *PLoS One* **8**, e70682 (2013).
124. R. Patalay, C. Talbot, Y. Alexandrov, M. O. Lenz, S. Kumar, S. Warren, I. Munro, M. A. Neil, K. König, P. M. French, "Multiphoton multispectral

fluorescence lifetime tomography for the evaluation of basal cell carcinomas," *PLoS One* **7**, e43460 (2012).
125. M. Manfredini, F. Arginelli, C. Dunsby, P. French, C. Talbot, K. König, G. Pellacani, G. Ponti, S. Seidenari, "High-resolution imaging of basal cell carcinoma: A comparison between multiphoton microscopy with fluorescence lifetime imaging and reflectance confocal microscopy," *Skin Res. Technol.* **19**, e433–e443 (2013).
126. M. Balu, C. B. Zachary, R. M. Harris, T. B. Krasieva, K. König, B. J. Tromberg, K. M. Kelly, "*In vivo* multiphoton microscopy of basal cell carcinoma," *JAMA Dermatol.* **151**, 1068–1074 (2015).
127. F. B. Legesse, A. Medyukhina, S. Heuke, J. Popp, "Texture analysis and classification in coherent anti-Stokes Raman scattering (CARS) microscopy images for automated detection of skin cancer," *Comput. Med. Imag. Graph.* **43**, 36–43 (2015).
128. M. Klemp, M. C. Meinke, M. Weinigel, H. J. Röwert-Huber, K. König, M. Ulrich, J. Lademann, M. E. Darvin, "Comparison of morphologic criteria for actinic keratosis and squamous cell carcinoma using *in vivo* multiphoton tomography," *Exp. Dermatol.* **25**(3), 218–222 (2016).
129. E. Dimitrow, M. Ziemer, M. J. Koehler, J. Norgauer, K. Konig, P. Elsner, M. Kaatz, "Sensitivity and specificity of multiphoton laser tomography for *in vivo* and *ex vivo* diagnosis of malignant melanoma," *J. Invest. Dermatol.* **129**(7), 1752–1758 (2009).
130. K. Hoffmann, M. Stucker, P. Altmeyer, K. Teuchner, D. Leupold, "Selective femotosecond pulse-excitation of melanin fluorescence in tissue," *J. Invest. Dermatol.* **116**, 629–630 (2001).
131. M. Balu, K. M. Kelly, C. B. Zachary, R. M. Harris, T. B. Krasieva, K. König, A. J. Durkin, B. J. Tromberg, "Distinguishing between benign and malignant melanocytic nevi by *in vivo* multiphoton microscopy," *Cancer Res.* **74**, 2688–2697 (2014).
132. H. Wang, S. Osseiran, V. Igras, A. J. Nichols, E. M. Roider, J. Pruessner, H. Tsao, D. E. Fisher and C. L. Evans, "*In vivo* coherent Raman imaging of the melanomagenesis-associated pigment pheomelanin," *Sci. Rep.* **6**, 37986 (2016).
133. G. Lentsch, M. Balu, J. Williams, S. Lee, R. M. Harris, K. König, A. Ganesan, B. J. Tromberg, N. Nair, U. Santhanam, "*In vivo* multiphoton microscopy of melasma," *Pigm. Cell Melanoma Res.* **32**, 403–411 (2019).
134. G. Lentsch, M. Valdebran, I. Saknite, J. Smith, K. G. Linden, K. König, R. J. Barr, R. M. Harris, B. J. Tromberg, A. K. Ganesan, "Non-invasive optical biopsy by multiphoton microscopy identifies the live morphology of common melanocytic nevi," *Pigm. Cell Melanoma Res.* **33**, 869–877 (2020).
135. G. Chen, J. Chen, S. Zhuo, S. Xiong, H. Zeng, X. Jiang, R. Chen, S. Xie, "Nonlinear spectral imaging of human hypertrophic scar based on two-photon excited fluorescence and second-harmonic generation," *Br. J. Dermatol.* **161**, 48–55 (2009).
136. V. Da Costa, R. Wei, R. Lim, C. H. Sun, J. J. Brown, B. J. Wong, "Nondestructive imaging of live human keloid and facial tissue using multiphoton microscopy," *Arch. Facial Plastic Surg.* **10**, 38–43 (2008).
137. M. B. Brewer, A. Yeh, B. A. Torkian, C. H. Sun, B. J. Tromberg, B. J. Wong, "Multiphoton imaging of excised normal skin and keloid scar: Preliminary investigations," *Proc. SPIE* **5312**, 204–208 (2004).
138. K. Lu, S. Zhuo, Z. Hong, G. Chen, X. Jiang, L. Zheng, J. Chen, "Non-linear spectral imaging microscopy studies of human hypertrophic scar," *J. Innov. Opt. Health Sci.* **2**, 61–66 (2009).
139. X. Zhu, S. Zhuo, L. Zheng, K. Lu, X. Jiang, J. Chen, B. Lin, "Quantified characterization of human cutaneous normal scar using multiphoton microscopy," *J. Biophoton.* **3**, 108–116 (2010).
140. X. Zhu, S. Zhuo, L. Zheng, X. Jiang, J. Chen, B. Lin, "Quantification of scar margin in keloid different from atrophic scar by multiphoton microscopic imaging," *Scanning* **33**, 195–200 (2011).
141. K. Lu, J. Chen, S. Zhuo, L. Zheng, X. Jiang, X. Zhu, J. Zhao, "Multiphoton laser scanning microscopy of localized scleroderma," *Skin Res. Technol.* **15**(4), 489–495 (2009).
142. J. H. Lee, S. Y. Chen, C. H. Yu, S. W. Chu, L. F. Wang, C. K. Sun, B. L. Chiang, "Noninvasive in vitro and *in vivo* assessment of epidermal hyperkeratosis and dermal fibrosis in atopic dermatitis," *J. Biomed. Opt.* **14**, 014008 (2009).
143. A. Uchugonova, R. M. Hoffman, M. Weinigel, K. Koenig, "Watching stem cells in the skin of living mice noninvasively," *Cell Cycle* **10**, 2017–2020 (2011).
144. A. Uchugonova, W. Cao, R. M. Hoffman, K. Koenig, "Comparison of label-free and GFP multiphoton imaging of hair follicle-associated pluripotent (HAP) stem cells in mouse whiskers," *Cell Cycle* **14**, 3430–3433 (2015).
145. D. Kapsokalyvas, R. Cicchi, N. Bruscino, D. Alfieri, F. Prignano, D. Massi, T. Lotti, F. S. Pavone, "*In-vivo* imaging of psoriatic lesions with polarization multispectral dermoscopy and multiphoton microscopy," *Biomed. Opt. Exp.* **5**, 2405–2419 (2014).
146. M. J. Koehler, K. Konig, P. Elsner, R. Buckle, M. Kaatz, "*In vivo* assessment of human skin aging by multiphoton laser scanning tomography," *Opt. Lett.* **31**, 2879–2881 (2006).

147. M. J. Koehler, A. Preller, N. Kindler, P. Elsner, K. König, R. Bückle, M. Kaatz, "Intrinsic, solar and sunbed-induced skin aging measured *in vivo* by multiphoton laser tomography and biophysical methods," *Skin Res. Technol.* **15**, 357–363 (2009).
148. S. Puschmann, C.-D. Rahn, H. Wenck, S. Gallinat, F. Fischer, "Approach to quantify human dermal skin aging using multiphoton laser scanning microscopy," *J. Biomed. Opt.* **17**, 0360051–0360056 (2012).
149. M. J. Koehler, S. Hahn, A. Preller, P. Elsner, M. Ziemer, A. Bauer, K. Konig, R. Buckle, J. W. Fluhr, M. Kaatz, "Morphological skin ageing criteria by multiphoton laser scanning tomography: Non-invasive *in vivo* scoring of the dermal fibre network," *Exp. Dermatol.* **17**, 519–523 (2008).
150. S. J. Lin, R. J. Wu, H. Y. Tan, W. Lo, W. C. Lin, T. H. Young, C. J. Hsu, J. S. Chen, S. H. Jee, "Evaluating cutaneous photoaging by use of multiphoton fluorescence and second-harmonic generation microscopy," *Opt. Lett.* **30**, 2275–2277 (2005).
151. S. Zhuo, X. Zhu, J. Chen, S. Xie, "Quantitative biomarkers of human skin photoaging based on intrinsic second harmonic generation signal," *Scanning* **35**, 273–276 (2013).
152. S. Wu, H. Li, H. Yang, X. Zhang, Z. Li, S. Xu, "Quantitative analysis on collagen morphology in aging skin based on multiphoton microscopy," *J. Biomed. Opt.* **16**, 040502–040502-3 (2011).
153. K. Sugata, O. Osanai, T. Sano, Y. Takema, "Evaluation of photoaging in facial skin by multiphoton laser scanning microscopy," *Skin Res. Technol.* **17**, 1–3 (2011).
154. H. Wang, T. Shyr, M. J. Fevola, G. O. Cula, G. N. Stamatas, "Age-related morphological changes of the dermal matrix in human skin documented *in vivo* by multiphoton microscopy," *J. Biomed. Opt.* **23**, 030501 (2018).
155. A.-M. Pena, T. Baldeweck, E. Decencière, S. Koudoro, S. Victorin, E. Raynaud, B. Ngo, P. Bastien, S. Brizion, E. Tancrède-Bohin, "*In vivo* multiphoton multiparametric 3D quantification of human skin aging on forearm and face," *Sci. Rep.* **12**, 1–19 (2022).
156. B. Yu, C.-Y. Dong, P. T. C. So, D. Blankschtein, R. Langer, "In vitro visualization and quantification of oleic acid induced changes in transdermal transport using two-photon fluorescence microscopy," *J. Invest. Dermatol.* **117**, 16–25 (2001).
157. B. Yu, K. Hean Kim, P. T. C. So, D. Blankschtein, R. Langer, "Topographic heterogeneity in transdermal transport revealed by high-speed two-photon microscopy: Determination of representative skin sample sizes," *J. Invest. Dermatol.* **118**, 1085–1088 (2002).
158. B. Yu, K. H. Kim, P. T. C. So, D. Blankschtein, R. Langer, "Visualization of oleic acid-induced transdermal diffusion pathways using two-photon fluorescence microscopy," *J. Invest. Dermatol.* **120**, 448–455 (2003).
159. K. Konig, J. Ehlers, F. Stracke, I. Riemann, "*In vivo* drug screening in human skin using femtosecond laser multiphoton tomography," *Skin Pharmacol. Physiol.* **19**, 78–88 (2006).
160. T. Richter, C. Peuckert, M. Sattler, K. Konig, I. Riemann, U. Hintze, K. P. Wittern, R. Wiesendanger, R. Wepf, "Dead but highly dynamic - the stratum corneum is divided into three hydration zones," *Skin Pharmacol. Physiol.* **17**, 246–257 (2004).
161. A. J. Mulholland, M. A. F. Kendall, N. White, B. J. Bellhouse, "Characterization of powdered epidermal vaccine delivery with multiphoton microscopy," *Phys. Med. Biol.* **49**, 5043–5058 (2004).
162. B. S. Grewal, A. Naik, W. J. Irwin, G. Gooris, C. J. de Grauw, H. G. Gerritsen, J. A. Bouwsra, "Transdermal macromolecular delivery: Real-time visualization of iontophoretic and chemically enhanced transport using two-photon excitation microscopy," *Pharm. Res.* **17**, 788–795 (2000).
163. J. Bender, C. Simonsson, M. Smedh, S. Engstrom, M. B. Ericson, "Lipid cubic phases in topic drug delivery: Visualization of skin distribution using two-photon microscopy," *J. Control. Release* **129**, 163–169 (2008).
164. F. Stracke, B. Weiss, C.-M. Lehr, K. Konig, U. F. Schaefer, M. Schneider, "Multiphoton microscopy for the investigation of dermal penetration of nanoparticle-borne drugs," *J. Invest. Dermatol.* **126**, 2224–2233 (2006).
165. K. Schenke-Layland, I. Riemann, O. Damour, U. A. Stock, K. Konig, "Two-photon microscopes and *in vivo* multiphoton tomographs-powerful diagnositc tools for tissue engineering and drug delivery," *Adv. Drug Deliv. Rev.* **58**, 878–896 (2006).
166. J. N. Lee, S. H. Jee, C. C. Chan, W. Lo, C. Y. Dong, S. J. Lin, "The effects of depilatory agents as penetration enhancers on human stratum corneum structures," *J. Invest. Dermatol.* **128**, 2240–2247 (2008).
167. B. Sarri, X. Chen, R. Canonge, S. Grégoire, F. Formanek, J.-B. Galey, A. Potter, T. Bornschlögl, H. Rigneault, "*In vivo* quantitative molecular absorption of glycerol in human skin using coherent anti-Stokes Raman scattering (CARS) and two-photon auto-fluorescence," *J. Control. Release* **308**, 190–196 (2019).
168. T. H. Tsai, S. H. Jee, J. Y. Chan, J. N. Lee, W. R. Lee, C. Y. Dong, "Visualizing laser-skin interaction *in vivo* by multiphoton microscopy," *J. Biomed. Opt.* **14**, 024034 (2009).

169. M. Koehler, K. Kellner, U. C. Hipler, M. Kaatz, "Acute UVB-induced epidermal changes assessed by multiphoton laser tomography," *Skin Res. Technol.* **21**, 137–143 (2015).
170. W. H. Jang, S. Shim, T. Wang, Y. Yoon, W.-S. Jang, J. K. Myung, S. Park, K. H. Kim, "*In vivo* characterization of early-stage radiation skin injury in a mouse model by two-photon microscopy," *Sci. Rep.* **6**, 19216 (2016).
171. G. Tian, H. Lui, J. Zhao, Z. Wu, S. Kalia, V. Richer, I. Seo, H. Ouyang, H. Zeng, "Tracking cellular dynamics of human skin responses to UV exposure using *in vivo* multimodal microscopy (Conference Presentation)," *Proc. SPIE* **10851**, 108510S (2019).
172. F. A. Navarro, P. T. C. So, R. Nirmalan, N. Kropf, F. Sakaguchi, C. S. Park, H. B. Lee, D. P. Orgill, "Two-photon confocal microscopy: A nondestructive method for studying wound healing," *Plast. Reconstr. Surg.* **114**, 121–128 (2004).
173. F. A. Navarro, P. T. C. So, A. Driessen, N. Kropf, C. S. Park, J. C. Huertas, H. B. Lee, D. P. Orgill, "Two photon confocal microscopy in wound healing," *Proc. SPIE* **4262**, 27–40 (2001).
174. A. Yeh, B. Kao, W. G. Jung, Z. Chen, J. S. Nelson, B. J. Tromberg, "Imaging wound healing using optical coherence tomography and multiphoton microscopy in an in vitro skin-equivalent tissue model," *J. Biomed. Opt.* **9**, 248–253 (2004).
175. B. A. Torkian, A. Yeh, R. Engel, C. H. Sun, B. J. Tromberg, J. F. Wong, "Modeling aberrant wound healing using tissue-engineered skin constructs and multiphoton microscopy," *Arch. Facial Plast. Surg.* **6**, 180–187 (2004).
176. J. Li, M. N. Wilson, A. J. Bower, M. Marjanovic, E. J. Chaney, R. Barkalifa, S. A. Boppart, "Video-rate multimodal multiphoton imaging and three-dimensional characterization of cellular dynamics in wounded skin," *J. Innov. Opt. Health Sci.* **13**, 2050007 (2020).
177. W. J. Mulholland, E. A. H. Arbuthnott, B. J. Bellhouse, J. F. Cornhill, J. M. Austyn, M. A. F. Kendall, Z. Cui, U. K. Tirlapur, "Multiphoton high-resolution 3D imaging of Langerhans cells and keratinocytes in the mouse skin model adopted for epidermal powdered immunization," *J. Invest. Dermatol.* **126**, 1541–1548 (2006).
178. R. N. Germain, M. J. Miller, M. L. Dustin, M. C. Nussenzweig, "Dynamic imaging of the immune system: Progress, pitfalls and promise," *Nat. Rev.* **6**, 497–507 (2006).
179. M. J. Miller, S. H. Wei, I. Parker, M. D. Cahalan, "Two-photon imaging of lymphocyte motility and antigen response in intact lymph node," *Science* **296**, 1869–1873 (2002).
180. B. Roediger, L. G. Ng, A. L. Smith, B. F. de St Groth, W. Weninger, "Visualizing dendritic cell migration within the skin," *Histochem. Cell Biol.* **130**, 1131–1146 (2008).
181. J. L. Li, C. C. Goh, J. L. Keeble, J. S. Qin, B. Roediger, R. Jain, Y. Wang, W. K. Chew, W. Weninger, L. G. Ng, "Intravital multiphoton imaging of immune responses in the mouse ear skin," *Nat. Protoc.* **7**, 221–234 (2012).
182. P. L. Tong, B. Roediger, N. Kolesnikoff, M. Biro, S. S. Tay, R. Jain, L. E. Shaw, M. A. Grimbaldeston, W. Weninger, "The skin immune atlas: Three-dimensional analysis of cutaneous leukocyte subsets by multiphoton microscopy," *J. Invest. Dermatol.* **135**, 84–93 (2015).
183. X.-N. Wang, N. McGovern, M. Gunawan, C. Richardson, M. Windebank, T.-W. Siah, H.-Y. Lim, K. Fink, J. L. Y. Li, L. G. Ng, "A three-dimensional atlas of human dermal leukocytes, lymphatics, and blood vessels," *J. Invest. Dermatol.* **134**, 965–974 (2014).
184. N. McGovern, A. Schlitzer, M. Gunawan, L. Jardine, A. Shin, E. Poyner, K. Green, R. Dickinson, X.-N. Wang, D. Low, "Human dermal CD14+ cells are a transient population of monocyte-derived macrophages," *Immunity* **41**, 465–477 (2014).
185. N. McGovern, A. Schlitzer, M. Gunawan, L. Jardine, A. Shin, E. Poyner, K. Green, R. Dickinson, X.-N. Wang, D. Low, "Population of monocyte-derived macrophages," *Immunity* **42**, 391 (2015).
186. M. J. Pittet, R. Weissleder, "Intravital imaging," *Cell* **147**, 983–991 (2011).
187. K. Konig, H. Liang, M. W. Berns, B. J. Tromberg, "Cell damage by near-IR microbeams," *Nature* **377**, 20–21 (1995).
188. K. Konig, H. Liang, M. W. Berns, B. J. Tromberg, "Cell damage in near-infrared multimode optical traps as a result of multiphoton absorption," *Opt. Lett.* **21**, 1090–1092 (1996).
189. K. Konig, P. T. C. So, W. W. Mantulin, E. Gratton, "Cellular response to near-infrared femtosecond laser pulses in two-photon microscopes," *Opt. Lett.* **22**, 135–136 (1997).
190. K. Konig, T. W. Becker, P. Fischer, I. Riemann, K. J. Halbhuber, "Pulse-length dependence of cellular response to intense near-infrared laser pulse in multiphoton microscopes," *Opt. Lett.* **24**, 113–115 (1999).
191. C. H. Sun, S. W. Chu, S. Y. Chen, T. H. Tsai, T. M. Liu, C. Y. Lin, H. J. Tsai, "Higher harmonic generation microscopy for developmental biology," *J. Struct. Biol.* **147**, 19–30 (2004).
192. I. H. Chen, S. W. Chu, C. K. Sun, B. L. Lin, P. C. Cheng, "Wavelength dependenct damage in biological multi-photon confocal microscopy: A micro-

spectroscopic comparison between femtosecond Ti: sapphire and Cr:forsterite laser sources," *Opt. Quantum. Electron.* **34**, 1251–1266 (2002).
193. B. R. Masters, P. T. C. So, C. Buehler, N. Barry, J. D. Sutin, W. W. Mantulin, E. Gratton, "Mitigating thermal mechanical damage potential during two-photon dermal imaging," *J. Biomed. Opt.* **9**, 1265–1270 (2004).
194. A. Vogel, J. Noack, G. Huttmann, G. Paltauf, "Femtosecond-laser-produced low-density plasmas in transparent biological media: A tool for the creation of chemical, thermal and thermomechanical effects below the optical breakdown threshold," *Proc. SPIE* **4633A**, 1–15 (2002).
195. A. Hopt, E. Neher, "Highly nonlinear photodamage in two-photon fluorescence microscopy," *Biophys. J.* **80**, 2029–2036 (2001).
196. F. Fischer, B. Volkmer, S. Puschmann, R. Greinert, W. Breitbart, J. Kiefer, R. Wepf, "Risk estimation of skin damage due to ultrashort pulsed, focused near-infrared laser irradiation at 800 nm," *J. Biomed. Opt.* **13**, 041320 (2008).
197. F. Fischer, B. Volkmer, S. Puschmann, R. Greinert, W. Breitbart, J. Kiefer, R. Wepf, "Assessing the risk of skin damage due to femtosecond laser irradiation," *J. Biophoton.* **1**, 470–477 (2008).
198. H. Wang, S. Zandi, A. Lee, J. Zhao, H. Lui, D. I. McLean, H. Zeng, "Imaging directed photothermolysis through two-photon absorption demonstrated on mouse skin–a potential novel tool for highly targeted skin treatment," *J. Biophoton.* **7**, 534–541 (2014).
199. Y. Huang, H. Lui, J. Zhao, Z. Wu, H. Zeng, "Precise spatially selective photothermolysis using modulated femtosecond lasers and real-time multimodal microscopy monitoring," *Theranostics* **7**, 513–522 (2017).
200. Y. Huang, Z. Wu, H. Lui, J. Zhao, S. Xie, H. Zeng, "Precise closure of single blood vessels via multiphoton absorption-based photothermolysis," *Sci. Adv.* **5**, eaan9388 (2019).
201. S. Tang, T. B. Krasieva, Z. Chen, B. J. Tromberg, "Combined multiphoton microscopy and optical coherence tomography using a 12-fs broadband source," *J. Biomed. Opt.* **11**, 020502 (2006).
202. S. Tang, C. H. Sun, T. B. Krasieva, Z. Chen, B. J. Tromberg, "Imaging subcellular scattering contrast by using combined optical coherence and multiphoton microscopy," *Opt. Lett.* **32**, 503–505 (2007).
203. Y. Yu, A. Lee, H. Wang, J. Zhao, S. Tang, H. Lui, D. I. McLean, H. Zeng, "New multimodal multiphoton imaging and spectroscopy apparatus for dermatology," *Proc. SPIE* **7548**, 75480N (2010).
204. S. Tang, J. Liu, T. B. Krasieva, Z. Chen, B. J. Tromberg, "Developing compact multiphoton system using femtosecond fiber lasers," *J. Biomed. Opt.* **14**, 030508 (2009).
205. S. Tang, W. Jung, D. McCormick, T. Xie, J. Su, Y.-C. Ahn, B. J. Tromberg, Z. Chen, "Design and implementation of fiber-based multiphoton endoscopy with microelectromechanical systems scanning," *J. Biomed. Opt.* **14**, 034005 (2009).
206. H. Bao, J. Allen, R. Pattie, R. Vance, M. Gu, "Fast handheld two-photon fluorescence microendoscope with a 475 um × 475 um field of view for *in vivo* imaging," *Opt. Lett.* **33**, 1333–1335 (2008).
207. G. Liu, T. Xie, I. V. Tomov, J. Su, L. Yu, J. Zhang, B. J. Tromberg, Z. Chen, "Rotational multiphoton endoscopy with a 1 um fiber laser system," *Opt. Lett.* **34**, 2249 (2009).
208. Y. Wu, Y. Leng, J. Xi, X. Li, "Scanning all-fiber-optic endomicroscopy system for 3D nonlinear optical imaging of biological tissues," *Opt. Exp.* **17**, 7907–7915 (2009).
209. Y. Zhao, M. Sheng, L. Huang, S. Tang, "Design of a fiber-optic multiphoton microscopy handheld probe," *Biomed. Opt. Exp.* **7**, 3425–3437 (2016).